Atmos. Chem. Phys. Discuss., 12, 8823–8855, 2012
www.atmos-chem-phys-discuss.net/12/8823/2012/
doi:10.5194/acpd-12-8823-2012

Atmospheric Chemistry and Physics Discussions

Investigation of source attributions of pollution to the Western Arctic during the NASA ARCTAS field campaign

H. Bian[1,2], P. Colarco[2], M. Chin[2], G. Chen[3], A. R. Douglass[2], J. M. Rodriguez[2], Q. Liang[4,2], J. Warner[1], D. A. Chu[1,2], J. Crounse[5], M. J. Cubison[6], A. da Silva[2], J. Dibb[7], G. Diskin[3], H. E. Fuelberg[8], G. Huey[9], J. L. Jimenez[6], Y. Kondo[10], J. E. Nielsen[11,2], S. Pawson[2], and Z. Wei[1]

[1]Joint Center for Environmental Technology UMBC, Baltimore, MD, USA
[2]Laboratory for Atmospheres, NASA Goddard Space Flight Center, Greenbelt, MD, USA
[3]NASA Langley Research Center, VA, USA
[4]Universities Space Research Association, GESTAR, Columbia, MD, USA
[5]California Institute of Technology, Pasadena, CA, USA
[6]Department of Chemistry and Biochemistry and CIRES, University of Colorado at Boulder, Boulder, CO, USA
[7]University of New Hampshire, Durham, NH, USA
[8]Department of Meteorology, Florida State University, Tallahassee, FL, USA
[9]School of Earth and Atmospheric Sciences, Georgia Institute of Technology, Atlanta, Georgia, USA

[10]University of Tokyo, Tokyo, Japan
[11]Science Systems and Applications Inc, Lanham, MD, USA

Received: 10 February 2012 – Accepted: 27 March 2012 – Published: 5 April 2012

Correspondence to: H. Bian (huisheng.bian@nasa.gov)

Published by Copernicus Publications on behalf of the European Geosciences Union.

Abstract

We present analysis of simulations using the NASA GEOS-5 chemistry and transport model to quantify contributions from different continents to the Western Arctic pollution, to investigate pollution sources and to identify transport pathways. We compare DC-8 airborne measurements of CO, SO_2, BC and SO_4 from the NASA Arctic Research of the Composition of the Troposphere from Aircraft and Satellites (ARCTAS) field campaigns (spring and summer, 2008) and observations from the AIRS instrument on NASA's Aqua satellite to demonstrate the strengths and limitations of our simulations and to support this application of the model. Comparisons of measurements along the flight tracks with regional averages show that the along-track measurements are representative of the region in April but not in July. Our simulations show that most Arctic pollutants are due to Asian anthropogenic emissions during April. Boreal biomass burning emissions and Asian anthropogenic emissions are of similar importance in July. European sources make little contribution to pollution in the campaign domain during either period. The most prevalent transport pathway of the tracers is from Asia to the Arctic in both April and July, with the transport efficiency stronger in spring than in summer.

1 Introduction

Midlatitude pollutants are often transported to the Arctic (Barrie, 1986; Heintzenberg, 1989; Weber et al., 2003), a region also vulnerable to climate change (Chapin et al., 1992). The Arctic serves as an important indicator of remote environmental changes because the effects of pollution from distant sources are clearly discernible. A series of Arctic field campaigns were conducted during the year 2008 to better understand pollution's impact on the Arctic and its feedback on climate. Here we use observations from the NASA Arctic Research of the Composition of the Troposphere from Aircraft and Satellites (ARCTAS) field campaigns (Jacob et al., 2010). ARCTAS Phase-A was based

ACPD
12, 8823–8855, 2012

in Fairbanks Alaska, USA in April and ARCTAS Phase-B (ARCTAS-B) was based at Cold Lake, Alberta, Canada in July.

Most of pollutants found in Arctic air have been transported from middle latitudes, and a large fraction is attributable to anthropogenic emissions. It is necessary to quantify the sources of pollution and identify the transport pathways in order to develop effective control strategies. Previous studies identified European emissions as the main source of Arctic pollution (Barrie, 1986; Rahn, 1981; Raatz and Shaw, 1984; Quinn et al., 2007, 2008; Shaw, 1995). However, recent investigations suggest that Asian emissions are critical, but the degree of importance is still subject to debate (Fisher et al., 2010; Koch and Hansen, 2005; Shindell et al., 2008; Singh et al., 2010; Stohl, 2006). The uncertainty of the sources is partially due to contradictory identification of complicated pathways for transport of air from mid-latitudes to Arctic and partially due to the rapid changes in the distribution of middle latitudes sources of industrial emissions in the past ~ 30 yr.

Based on analysis of snow samples, Hegg et al. (2009) conclude that more than 90 % of the black carbon (BC) deposited in the Arctic in spring is due to biomass burning, another important source of Arctic pollution. Fires from Russia, Eastern Europe, and Central Asia all have their imprint on the Arctic (Stohl et al., 2007; Warneke et al., 2009, 2010). However, unlike anthropogenic sources that are basically all from outside the Arctic, local boreal forest fires make important contributions to the total emissions from biomass burning.

A series of ARCTAS-related studies were published recently to address the source contribution to the Arctic with highlights on anthropogenic and biomass burning impacts. By tracking trajectories, Harrigan et al. (2011) studied the mean transport characteristics in ARCTAS-A from anthropogenic emissions. A global chemistry and transport model GEOS-CHEM was used to interpret the ARCTAS-A measurements and to investigate the Arctic spring CO (Fisher et al., 2010), sulfate-ammonium aerosols (Fisher et al., 2011), and BC and organic aerosol (Wang et al., 2011). These studies all indicated that Asian anthropogenic and biomass burning emissions are impor-

ACPD
12, 8823–8855, 2012

tant sources for the Arctic spring pollution. Additional studies solely used aircraft measurements in investigating pollution emissions, transport, atmospheric composition and chemistry, and pollution spatial variation (Cubison et al., 2011; Hecobian et al., 2011; Kondo et al., 2011a; Matsui et al., 2011a, b; McNaughton et al., 2011; Shinozuka et al., 2011a, b; Singh et al., 2010). To date, there has been no comprehensive modeling study exploring source attribution for the Western Arctic during both the ARCTAS-A and ARCTAS-B periods. A model is necessary because the aircraft measurements alone are not sufficient for the Arctic regional wide pollution during ARCTAS-B, a major conclusion of the present work.

This study focuses on the impact of long-range transport and boreal forest fires on the Western Arctic during both ARCTAS-A and ARCTAS-B. Simulations using tagged tracers in the GEOS-5 model (Bian et al., 2010) are used to quantify the contributions from continental sources and biomass burning to regional pollution. Evaluation of the simulations using observations from ARCTAS and from the AIRS instrument on NASA's Aqua satellite supports this use of the model and the conclusions drawn in the work. Integrated analysis of carbon monoxide (CO), sulfur dioxide (SO_2), black carbon (BC) and sulfate aerosols (SO_4), all measured by the NASA DC-8 and simulated by the GEOS-5 model, provides insight into the objectives of this paper. Carbon monoxide is not subject to dry and wet removals but can be oxidized by reaction with hydroxyl (OH) leading to net production of ozone (O_3) (Bian et al., 2007). Both anthropogenic and biomass burning emissions contribute to CO. The lifetime of tropospheric CO is on the order of months (Pan et al., 1995), making it a good tracer for investigating hemispheric long-range transport. Black carbon, an important agent in Arctic climate change (Flanner et al., 2007), can also be emitted from anthropogenic and biomass burning emissions. Tropospheric BC experiences dry and wet scavenging with a lifetime of approximately one week (Koch and Hansen, 2005). Black carbon is a useful tracer to investigate pollution source because transcontinental transport and transport from Northern Hemisphere (NH) middle latitudes to the Arctic typically occurs on timescale of days to weeks. Given these similarities and differences, the ratio of BC to CO con-

ACPD
12, 8823–8855, 2012

tains information about pollutant emissions as well as atmospheric dry and wet removal processes.

The gas SO_2 is a precursor for sulfate particles (SO_4); this pair of tracers is also useful in pursuing our objectives. Unlike the BC and CO combination, which have no direct chemical connection, atmospheric SO_4 is primarily produced by the chemical oxidation of SO_2, which is mainly directly emitted into the atmosphere from fossil fuel combustion and volcanoes, with smaller contributions from the oxidation of naturally emitted tracers such as dimethyl sulphide (DMS) (Chin et al., 2002). Because SO_4 is produced from SO_2, the ratio of SO_2 to SO_4 contains information about air mass age and photochemical processes that take place during transport.

We describe the NASA DC-8 measurements, AIRS CO retrievals, and NASA GEOS-5 model simulations during the ARCTAS period in Sect. 2. The GEOS-5 model results are compared with the ARCTAS observations in Sect. 3 where we also show that aircraft measurements from ARCTAS-B are not representative of pollution on a regional spatial scale. To support our use of simulations to quantify regional sources of pollution, we evaluate the model simulations using ARCTAS measurements and AIRS satellite observations, paying careful attention to two case studies. In Sect. 4 we use GEOS-5 simulations to investigate sources, transport, and transformation of Arctic pollutants during the ARCTAS periods. The conclusions and further discussions are given in Sect. 5.

2 Observations and GEOS-5 model

2.1 CO and aerosols from aircraft measurements

The measurements of CO, BC, SO_2, and SO_4 from NASA DC-8 aircraft (http://www-air.larc.nasa.gov/cgi-bin/arcstat-c are used to evaluate satellite CO retrievals and model simulation. There were 11 flights during March-April over Alaska and 7 flights in July over Canada. The gas tracer CO was measured using Tunable Diode Laser Absorp-

ACPD
12, 8823–8855, 2012

tion Spectroscopy (TDLAS), which provides fast-response (~ 1 s) and high-precision (±1 part per billion by volume) measurements (Diskin et al., 2002; Sachse et al., 1987). Aerosol BC was measured using a Single Particle Soot Photometer (SP2) based on Laser-Induced Incandescence (LII) with high accuracy and temporal resolution (Kondo et al., 2011b; Moteki and Kondo, 2007). The absolute accuracy of the BC measurements is estimated to be 10 % (Kondo et al., 2011a). There were two SO_2 instruments and two SO_4 instruments onboard the DC-8. Both the California Institute of Technology (CIT) team and the Georgia Institute of Technology (GIT) team used Chemical Ionization Mass Spectroscopy (CIMS) with a 1 s integration period for SO_2 measurement (Huey et al., 2004; Salcedo et al., 2004; Slusher et al., 2004). For SO_4, the University of New Hampshire (UNH) team used Soluble Acidic Gases and Aerosol (SAGA), a slower mist chamber/ion chromatography technique (Scheuer et al., 2003) and the University of Colorado-Boulder (UCB) team used high-resolution Aerosol Mass Spectrometry (AMS) with 12 s data intervals (Dunlea et al, 2009).

Fast response aircraft data were averaged to 1-min intervals along the flight tracks, and slow response data were interpolated to the same intervals (http://www-air.larc.nasa.gov/cgi-bin/arcstat-c).

2.2 Satellite data of CO from Atmospheric Infrared Sounder (AIRS)

The AIRS, one of the instruments onboard Aqua (launched in 2002), makes measurements relevant to climate and air quality monitoring (Aumann et al., 2003). CO retrievals are obtained from the 2160–2200 cm^{-1} portion of the spectrum on the edge of the 1–0 vibration-rotation band of CO with a spectral spacing of ~1.8 cm^{-1} and an instrument Noise Equivalent Differential Temperature (NeDT) of typically 0.14 K (McMillan et al., 2005). AIRS measures across a 1600 km wide swath and cloud clearing recovers up to 80 % of cloudy coverage, thereby obtaining global coverage approximately twice per day (Susskind et al., 2003). AIRS CO products have been improved during the years since launch (Susskind et al., 2003; McMillan et al., 2010; Warner et al., 2007, 2010). For example, the AIRS operational CO products agree with in situ measurement of

ACPD
12, 8823–8855, 2012

the NASA Intercontinental Chemical Transport Experiment-North America (INTEX-NA) to 10 % for V4 (Warner et al., 2007) and 6–10 % for V5 (McMillan et al., 2010). We use the AIRS CO product retrieved with the Optimal Estimation (OE) method (Warner et al., 2010). This product demonstrates an overall better agreement (5–15 % in the low troposphere) with field campaign measurements.

2.3 GEOS-5 model simulation

CO and aerosol distributions for the entire ARCTAS campaign period were simulated using the NASA Goddard Earth Observing System model, version 5 (GEOS-5) in a "replay" mode as described below.

GEOS-5 is a global Earth system model, containing components for atmospheric circulation and composition, ocean circulation and biogeochemistry, land surface processes and data assimilation (Rienecker et al., 2008). A module of the Goddard Chemistry, Aerosol, Radiation, and Transport model (GOCART; Chin et al., 2002) was used to simulate processes of source, sink, transportation, and transformation for both CO and aerosols within the GEOS-5 system. GOCART aerosols included dust, sea salt, sulfate, black carbon, and organic matter mixed externally (non-interacting). In this study, GOCART CO was decomposed into tagged CO tracers, each designed to track a particular emission type or emissions from a particular region. Sources and oxidant fields for CO and aerosol simulations were described in Bian et al. (2007) and Colarco et al. (2010) with several updates. Anthropogenic aerosol and trace gas precursor sources are specified primarily from the AeroCom inventory (Diehl, 2011). Daily, gridded biomass burning emissions of aerosols, SO_2, and CO are prescribed as a function of fire radiative power observed from the space-based Moderate Resolution Imaging Spectroradiometers.

The model has 72 hybrid vertical sigma levels which are terrain following near the surface and transition to pressure levels above about 100 hPa with a model top at 0.01 hPa (about 85 km). The model was run at $0.5^{\circ} \times 0.625^{\circ}$ latitude × longitude horizontal resolution. The model is "replayed" from the Modern Era Retrospective-Analysis

ACPD
12, 8823–8855, 2012

for Research and Applications (MERRA) meteorological analyses produced by NASA Global Modeling and Assimilation Office (Rienecker et al., 2011). Every six hours the model dynamical state (winds, pressure, temperature, and humidity) is set to the balanced state provided by MERRA and then a six-hour forecast is performed until the next analysis is available.

The five tagged CO tracers shown in Fig. 1a are important to the Arctic background environment and episodic events based on previous studies (Bian et al., 2010; Fisher et al., 2010; Fuelberg et al., 2010; Stohl, 2006). These five types are: three anthropogenic emissions from North America (NAFF, yellow F1), Asia (ASFF, orange F2), and Europe (EUFF, green F3), and two biomass burning emissions from non-boreal regions (NBBB, blue-shaded area B1) and boreal regions (BOBB, non-blue-shaded area B2). Figure 1b, c shows the DC-8 flight tracks for all flights in ARCTAS-A and ARCTAS-B, respectively.

3 Representation of aircraft measurement and model validation

3.1 Need for a 3-D model to study Western Arctic pollution sources

The representation of the aircraft measurements for Arctic regional wide pollution is explored here to indentify the best tool and dataset for the study of source attribution to the Western Arctic.

Vertical distributions of CO volume mixing ratios from DC-8 measurement and GEOS-5 simulation are shown in Fig. 2a, b (top panel) for the GEOS-5 data averaged over the Arctic area of 50–90° N and 40–170° W and in Fig. 2c, d (bottom panel) for the model output sampled at the measurement time and location. In this figure, the DC-8 1-min merged product is also averaged vertically within 1 km layers, and the mean and standard deviation are shown as red lines. The GEOS-5 total and tagged CO volume mixing ratios are also vertically averaged. The CO other than the aforementioned five tagged categories is designated as "Other CO".

ACPD
12, 8823–8855, 2012

Ideally, we would like to use aircraft measurements to study the pollution for the Arctic region. Figure 2a, b indicates that we can do so in April but not in July since the DC-8 measurements poorly represent the regional wide CO distribution in July. An alternative tool is a 3-D model if it reproduces the observations. We therefore evaluate the GEOS-5 model replay simulation using ARCTAS-A and ARCTAS-B DC-8 measurements and AIRS retrievals of CO to get confidence in this use of the model.

Unlike the measurements that give overall tracer information with mixed source origins and types, the GEOS-5, like many other models, produces detailed information of CO source regions and types via CO tags. This model feature is needed for this study of source attribution to the Arctic.

3.2 Model validation

3.2.1 Case studies

We first investigate two flights to evaluate the GEOS-5 model performance and to closely examine the air inside and outside plumes (case 1) and in the different environments sampled during the flights (case 2).

Figure 3 shows CO, BC, SO_2, and SO_4 sampled on 8 July from Cold Lake, Canada to Thule, Greenland (flight 21). The pollutant distributions and plume transport pathways are shown on Fig. 3a using CO volume mixing ratios at 400 hPa from the GEOS-5 simulation, the level where the plumes were located. GEOS-5 gives similar plume patterns as shown by comparison with the AIRS column CO retrieval (Fig. 3b). Note that we use the AIRS OE CO total column amount because it is not possible to vertically resolve CO layer information because AIRS has approximately one Degree of Freedom for Signals (DOFS) in the free troposphere. Curtain plots of the tagged CO to its major sources boreal biomass burning (BOBB) and Asia fossil fuel (ASFF) are shown in Fig. 3c. Figure 3d–g shows curtain plots of the GEOS-5 CO, BC, SO_2, and SO_4 respectively (left of the panels) and their concentrations along the flight tracks from observation and simulation (right).

ACPD
12, 8823–8855, 2012

This particular flight encountered two plumes, one over the US-Canada border and the other over the Arctic near Greenland. Analysis of the atmospheric circulation indicated that the jet stream had retreated north into the middle latitudes and had two components over Asia. The southern segment passed over Central Asia and was near the climatological position, while the component over extreme Northern Asia was $\sim 10\,m\,s^{-1}$ stronger than its weaker climatological counterpart (Fig. 16 in Fuelberg et al., 2010). Ten day back trajectories from the aircraft tracks show that both the southern and northern plumes came from Asia and its surrounding areas. Specifically, the southern plume originated from Asia and Eurasia and the north plume from northeast Asia and Labrador Sea (Fuelberg et al., 2010, http://fuelberg.met.fsu.edu/research/arctas/traj/traj/html).

The tagged CO simulations, indicated by the various thin color lines on right column of Fig. 3d, show that the sampled CO concentration in the southern plume had comparable Asian industrial and boreal biomass burning pollutions, while the sampled CO in the northern plume was mainly due to Asian industrial pollution, consistent with the origin of the plumes analyzed by Fuelberg et al. (2010). To better understand the contributions from different source regions, the curtain plots of tagged CO from BOBB and ASFF are given in Fig. 3c. Although both emission sources contributed to the two plumes, their vertical impact regions differed slightly. The center of Asian anthropogenic impact was right above the center of boreal biomass burning impact. This is particularly true for the north CO plume so that the flight captured only ASFF at its flight altitude in the upper troposphere. This layering of plumes, i.e. the ASFF plume just above BOBB plume, was also observed by previous studies (Matsui et al., 2011a; Singh et al., 2010).

Vertically, the southern CO plume was located between 500–300 hPa, while the northern CO plume was slightly higher between 400–250 hPa, supporting the previous statistical analyses that the majority of tracers released from the NH reach 70° N at altitudes with pressures less than 400 hPa (e.g. 46.0 % for ARCTAS-B in Table 2, Fuelberg et al., 2010).

ACPD
12, 8823–8855, 2012

The two plumes were also evident in the distributions of the aerosol tracers. But instead of the aerosol enhancement shown in the southern plume, the aerosol concentrations were depleted in the northern plume. Specifically, SO_2 and SO_4 inside the northern plume were lost almost entirely, BC was lost partially, but CO was still greatly enhanced. This interesting phenomenon could be attributed to the transport trajectories since the northern plume passed through precipitation while the southern plume did not. In addition, the age of the northern plume was much older than the southern plume so tracers in the northern plume had a longer time to be removed via wet and, to a lesser extent, dry deposition. We checked model CO mixing ratios at 500 hPa backward from the flight day to trace the plumes' histories. We found that the southern plume moved eastward quickly and passed over the Pacific within 3–5 days. The northern plume slowly advanced northeast following a Pacific cyclone, taking more than 9 days to reach the ARCTAS domain, which is comparable to BC's lifetime.

Figure 4 shows results from a transit flight on July 13 from Cold Lake, Alberta, Canada, to Palmdale, California, USA (flight 24). The flight was chosen because it sampled very different air masses: relatively clean before waypoint 5 and polluted air afterward. Ten day back trajectories from the aircraft tracks indicate that four different source origins were sampled above 500 hPa before waypoint 5 – Northern Asia, near Japan, the Central Pacific Ocean, and off the coast of Baja California (Fig. 24a in Fuelberg et al., 2010). The aircraft descended when it headed into the polluted air during the rest of its journey. The 5-day back trajectories from the aircraft tracks indicate that the sampled air primarily came from California surface sources with supplement from the Eastern Pacific Ocean.

The GEOS-5 CO mixing ratios at 700 hPa and AIRS column CO are shown in Fig. 4a, b, respectively, with both indicating the plume sampled by the aircraft. Similarly, Fig. 4c–f shows curtain plots (left) and the model-observation comparisons of the tracer concentrations (right) along the flight for CO, BC, SO_2, and SO_4, respectively. Clearly, two distinct environment regimes were sampled along the flight track: one was the clean background environment from Cold Lake to Central Nevada (waypoints 1–5) and the

ACPD
12, 8823–8855, 2012

other was the local US polluted environment during the rest of the flight (waypoints 5–11). The tagged CO information (thin color lines on Fig. 4c right) indicates that Asian fossil fuel emissions dominated the Arctic background, while local biomass burning, and to a lesser extent the nearby industrial emission, dominated the US polluted environment.

The ratios of BC vs. CO (BC/CO) and SO_2 vs. SO_4 (SO_2/SO_4) sampled by the aircraft and simulated by GEOS-5 were calculated along the flight track and are shown in Fig. 4g, h. These ratios imply information for the evolution of plumes, air mass ages and origins. The older and cleaner the air is, the smaller the BC/CO and SO_2/SO_4 will be. This occurs because BC is removed from atmosphere much faster than CO due to a much shorter lifetime of BC. Eventually, much less BC than CO remains in an old clean air. Unlike the removal process being responsible for the change of BC/CO, the chemical transformation is the reason for the pattern of SO_2/SO_4. We know that the majority of sulfur emitted from industrial or biomass burning into atmosphere is in the form of SO_2, with only a few percent in SO_4 directly. The SO_2 is then oxidized to form SO_4 in the atmosphere. Therefore, the SO_2/SO_4 is greater in fresh polluted air and smaller when the air is older.

Figure 4g, h shows ratios of BC/CO and SO_2/SO_4 were significantly smaller in the clean Arctic air than in the US polluted air, consistent with what we expected. The modeled and observed BC/CO ratios were close to each other over US but not over the Arctic. This is because GEOS-5 did not remove enough BC, resulting in a much higher BC/CO than measured over the Arctic. Shindell et al. (2008) conducted multi-model comparisons of aerosol transport to the Arctic and showed large differences in the calculated BC concentrations in the Arctic by the different GCM models used in the HTAP report. They suggested that the large differences are likely due to the different treatments of aerosol aging from hydrophobic to hydrophilic and rainout/washout processes of aerosols during transport in the individual models rather than differences in dry deposition or local Arctic removal processes. GEOS-5 treats BC as hydrophobic and hydrophilic and removes efficiently only hydrophilic BC via wet scavenging. The

ACPD
12, 8823–8855, 2012

large differences in model and observed BC/CO ratios indicate the necessity of further improvements of GEOS-5's BC removal processes during long-range transport. Duplicate measurements were available for SO_2 and SO_4. We used AMS for SO_4 in Fig. 4h since the AMS has more specific and fast response techniques. Both CIT and GIT SO_2 are used to calculate SO_2/SO_4 and only the latter is shown in the figure for simplicity since the two are similar.

3.2.2 Overall validation

An overall model evaluation using all DC-8 flight measurements during ARCTAS-A and ARCTAS-B is given here. The evaluation is important for using the model with its tag tracers in the study of source attribution for the Arctic.

Figure 5 presents a composite of the DC-8 measured CO mixing ratios compared to the total CO mixing ratio simulated by the GEOS-5 model. Here, the model is sampled at the time and location where the aircraft measurements were made. A separate panel is presented for the spring and summer phases of the ARCTAS campaign, and within each panel the comparison points are color coded by the particular aircraft flight, consistent with the colored flight tracks shown in Fig. 1b, c.

The April campaign (ARCTAS-A) was conducted from Fairbanks, focusing on the long-range transport of Asian pollutants. Measured and modeled CO values seldom exceeded 200 ppbv, suggesting long-range transport rather than local sources as the origin of the observed CO. The model CO is well correlated with the observations ($r = 0.79$). The ratio of mean modeled CO to mean observed CO is 0.79, indicating an overall mean bias. This underestimation of CO at northern extratropical and high latitudes in spring is a general problem in current chemical transport models (Shindell et al., 2006; Fisher et al., 2010). One possible explanation is that the emission inventories for springtime Asian sources may underestimate emissions from residential fuel use and vehicle cold starts (Kopacz et al., 2010; Zhang et al., 2009).

The July campaign (ARCTAS-B) was based at Cold Lake, Canada. The area experienced large local fires, so that the observed CO could be over 1500 ppbv. The DC-8

ACPD
12, 8823–8855, 2012

sometimes observed very high CO values that were missed in the model simulation and vice versa. These high CO events not simulated in the model are possibly due to missing sources, the inability of the model to capture fine structure plumes, or plumes simply being misplaced in the model. The correlation of the model with the observations is thus reduced. The simulated mean CO underestimation is greater in July than in April.

Figure 2c, d shows the vertical distributions of CO volume mixing ratios from DC-8 measurement and GEOS-5 simulation with the model output sampled at the measurement time and location for ARCTAS-A and ARCTAS-B, respectively. The comparisons indicate that the model agrees well with the measurement along flight track when the compared samples further lumped together within 1 km vertically. This type of evaluation is particularly important for the study of regional wide Arctic pollution. The comparisons give us some confidences in using the GEOS-5 in the study.

4 Source attribution for the Western Arctic

Our ultimate goal is to understand the sources to regional wide Arctic pollution. We will show here the impact of emissions and transport on the Arctic environment using the GEOS-5 tag CO results.

The regional mean tag CO vertical distributions shown in Fig. 2a for ARCTAS-A indicate that the Western Arctic air is overwhelmingly impacted by ASFF from the surface to the upper troposphere, and this Asian contribution exceeds the overall contributions from NAFF and EUFF. Our results support the findings that Asian anthropogenic emissions are the dominant source of Arctic CO pollution in the troposphere in April (Fisher et al., 2010; Warneke et al., 2010). Overall biomass burning (BOBB + NBBB) and the "Other CO" contribute about 1/3 of the Western Arctic CO in April. The standard deviation is very small in the low Arctic atmosphere, indicating a relatively homogeneous CO environment. The regional CO mixing ratio is nearly constant from the surface to

ACPD
12, 8823–8855, 2012

the middle troposphere (around 5–6 km) and then gradually decreases with increasing altitude. The European contribution is confined to the low to middle troposphere.

During ARCTAS-B as shown in Fig. 2b, ASFF and BOBB are the most important sources of the Arctic pollution and EUFF contribution is very low. The contribution of ASFF to the Arctic mean CO is much less in summer than in April, which indicates that the transport efficiency from Asia to the Arctic is low in summer. Matsui et al. (2011a) also reported this less efficient summer transport, 4 % in summer and 80 % in spring, due to differences in the transport mechanisms and accumulated precipitation along trajectories. Carbon monoxide does not monotonically decrease with increasing altitude. There is a CO enhancement in the upper troposphere around 5–8 km, which indicates that pollutions from outside enter the Arctic most likely within this layer.

The Arctic is a receptor of pollutants transported from the northern mid-latitude continents. We use the five tagged CO tracers (Fig. 1a) to assess the origin of different pollutants in the Arctic and their source-receptor relationships. We sort the observed and GEOS-5 total CO according to the dominant CO tag for each data point along the aircraft flight track. Here dominant CO refers to the CO tag having the greatest value, as well as its value being not less than 40 % of the total CO. This approach has limitations when there is no clear dominant tag or if the model gives biased results. The probability distribution function (PDF) of modeled and observed total CO was calculated for each of the five source groups, four of which are shown in Fig. 6. The model simulated CO result sampled same as flight measurement is shown in red line and the model result averaged over the Western Arctic domain is shown in green shaded area. The EUFF tag was excluded from the figure since the sampled total CO was almost never dominated by the tagged European pollution. The numbers shown in Fig. 6 recorded the total minutes sampled for each group in each campaign.

One objective of ARCTAS was to find the contributions from different emission types. Our data indicate that the dominant type and origin (in terms of number of observations) of CO to the Arctic is ASFF in April and both ASFF and BOBB in July, same conclusion we observed from Fig. 2a, b. Our analysis indicates that biomass burning (BOBB +

ACPD
12, 8823–8855, 2012

NBBB) makes a noticeable contribution to the mean CO in July when the contribution of biomass burning could exceed ASFF. We found that the European FF source is generally a minor contributor to CO concentrations during ARCTAS. Previous studies indicate that European pollution is largely confined to regions around south of 60° N during negative phases of the North Atlantic Oscillation (NAO), but reaches roughly about 70° N during positive phases of the NAO (Eckhardt et al., 2003). The NAO index was −1.07, −1.73, −1.39, and −1.27 from April, May, June, and July, 2008, respectively (http://www.cpc.ncep.noaa.gov/products/precip/CWlink/pna/nao.timeseries.gif).

Figure 6 also implies qualitatively the age of the measured air masses and how polluted Arctic air would be due to each outstanding source and type. During ARCTAS-A, the Arctic air would be very clean if the majority of pollution came from NBBB (i.e. the probable total CO mixing ratio is very low). In this case, the air from non-boreal region must travel long distances before arriving in the Arctic. During ARCTAS-B, the CO PDFs show a longer tail toward higher CO compared to the spring distributions. This is pronounced when the pollutants were mostly from the biomass burning sources (BOBB and NBBB) with most severe episodes (CO > 350 ppbv), or from a relatively local anthropogenic source (NAFF) with frequently high Arctic CO (CO ~ 200 ppbv). In addition, the most probable CO from BOBB during July is less than during April although both local and Russian BB CO emissions during summer are larger than during spring. This indicates that the majority BOBB CO in summer was still attributed to Russian BB, and the transport efficiency of Russian BB air to the North Pole is less in summer than in spring. Matsui et al. (2011a) indicated that spring Russian BB air could sustain its pollutant to the Arctic due to its nearly isentropic slow ascent so that it was subjected to low accumulated precipitation removal. The same conclusion for the transport efficiency can be derived from the change of ASFF PDF and the conclusion is consistent with our analysis in Fig. 2.

Another campaign objective was to estimate the emissions from boreal forest fires and to investigate the near-field chemical evolution of the fire plume. MODIS data over Siberia from 2000–2009 indicated that fire counts during April 2008 were the highest

ACPD
12, 8823–8855, 2012

recorded during that period, while the summer peak was second only to 2003 (Singh et al., 2010). Canadian fires during ARCTAS-B were near their normal level (Soja et al., 2008), while California experienced one of the largest episodes of wildfires in summer 2008, with over 1000 fires (Singh et al., 2010). Episodes from all these biomass burning emissions were detected during the ARCTAS as shown in Fig. 6. In April, the Siberian fires were measured over Fairbanks so that BOBB gives highest probable CO. During July, California fires (i.e. NBBB) are most prominent over Canada as shown by the longer tail toward high CO. Local Canadian fires (i.e. BOBB) could cause extremely polluted episodes as shown by the small bumps at extremely high CO.

5 Conclusions

We analyzed CO, BC, SO_2, and SO_4 measured by the NASA DC-8 aircraft during the ARCTAS spring and summer campaigns in 2008. These data were used to evaluate the GEOS-5 model simulations. We examined overall consistency between satellite AIRS retrievals and GEOS-5 model simulation. We also applied the GEOS-5 simulations with tagged CO to interpret the ARCTAS flight measurements and to investigate potential pollutant sources, transport pathways, and their atmospheric evolution to the sampled regions by combining with the measurements.

The ARCTAS DC-8 measurements are representative of the regional Arctic pollution in ARCTAS-A (April), but not in ARCTAS-B (July). It will be misleading to use aircraft measurements to understand Arctic pollution in July. In this work, we use the GEOS-5 model simulation to investigate the Western Arctic pollution since the model and measurement agree well along flight tracks.

Our integrated analysis indicates that the mean of the Western Arctic CO in April is mostly impacted by ASFF (accounting more than 1/3 of the Arctic CO mean), during which biomass burning contributes roughly half of ASFF. In July, both ASFF and BOBB have comparable contributions to the mean CO. Biomass burning also makes a large contribution to the Arctic pollution variability in July. On the other hand, we found that

ACPD
12, 8823–8855, 2012

European sources seldom made important contributions to the CO during the campaign domain and period, perhaps because the NAO was negative.

Our results show that transport of Asian emissions is the most important transport pathway of CO and aerosol tracers to the Western Arctic throughout the troposphere during April, and in the middle-upper troposphere (5–8 km) during July, with stronger transport efficiency during spring than summer.

Two flights were examined in detail. The 8 July case indicated pollution originating from Asia that split into two components over the Pacific Ocean. The southern plume arrived at the US-Canada border and was relatively fresh with enhanced pollutants. The northern plume reached closer to the North Pole and was older, with almost all short-lived pollutants having been removed. In addition, the northern plume was slightly higher (400–250 hPa) in altitude than the southern plume (500–300 hPa), and the northern plume had separated ASFF and BOBB centers with ASFF located just above BOBB. These features were also observed in other plumes, and may represent general transport features during ARCTAS-B since they are consistent with the characteristics of the jet stream during ARCTAS-B (Fuelberg et al., 2010).

We also analyzed ratios of BC/CO and SO_2/SO_4 along a specific flight (13 July) as proxies of the age of polluted air during atmospheric evolution. The BC/CO and SO_2/SO_4 calculated by DC-8 measurements were much higher in freshly polluted air near its source regions ($1.8 \pm 0.4\,\mathrm{ng\,sm^{-3}\,ppbv^{-1}}$ for BC/CO and $510 \pm 256\,\mu\mathrm{g\,m^{-3}\,ppbv^{-1}}$ for SO_2/SO_4) and lower in old clean air over remote ocean regions ($0.032 \pm 0.028\,\mathrm{ng\,sm^{-3}\,ppbv^{-1}}$ for BC/CO and $93 \pm 39\,\mu\mathrm{g\,m^{-3}\,ppbv^{-1}}$ for SO_2/SO_4). These patterns can be understood given that BC has a much shorter lifetime than CO and SO_4 is produced from SO_2 in the atmosphere.

The comparisons between the measurement and the simulation indicate that the model simulates long distance transport of air pollution tracers, but does not entirely represent emissions from boreal forest fires spatially or temporally. The model underestimated CO during both phases of ARCTAS, most likely due to an underestimate of

ACPD
12, 8823–8855, 2012

sources from residential fuel use and vehicle cold starts during the spring phase and missing local boreal biomass burning sources during the summer phase.

Supplementary material related to this article is available online at: http://www.atmos-chem-phys-discuss.net/12/8823/2012/acpd-12-8823-2012-supplement.pdf.

Acknowledgement. The authors thank Hanwant, B. Singh and Erin P. Czech for their helpful discussion. This work was supported by the NASA ARCTAS program and the NASA MAP (NNH08ZDA001N) program. JLJ and MJC were supported by NASA NNX08AD39G.

References

Aumann, H. H., Chahine, M. T., Gautier, C., Goldberg, M., Kalnay, E., McMillin, L., Revercomb, H., Rosenkranz, P. W., Smith, W. L., Staelin, D., Strow, L., and Susskind, J.: AIRS/AMSU/HSB on the aqua mission: design, science objectives, data products and processing systems, IEEE T. Geosci. Remote Sens., 41, 253–264, 2003.

Barrie, L.: Arctic air pollution: an overview of current knowledge, Atmos. Envir., 20, 643–663, 1986.

Bian, H., Chin, M., Kawa, R., Duncan, B., Arellano Jr., A., and Kasibhatla, R.: Uncertainty of global CO simulations constraint by biomass burning emissions, J. Geophys. Res., 112, D23308, doi:10.1029/2006JD008376, 2007.

Bian, H., Chin, M., Kawa, S. R., Yu, H., Diehl, T., and Kucsera, T.: Multiscale carbon monoxide and aerosol correlations from satellite measurements and the GOCART model: implication for emissions and atmospheric evolution, J. Geophys. Res., 115, D077302, doi:10.1029/2009JD012781, 2010.

Chapin III, F. S., Jefferies, R., Reynolds, R., Shaver G., and Svoboda, J. (ed.): Arctic ecosystems in a changing climate: an ecophysiological perspective, Academic Press, New York, NY, USA, 469 pp., 1992.

Chin, M., Ginoux, P., Kinne, S., Torres, O., Holben, B. N., Duncan, B. N., Martin, R. V., Logan, J. A., Higurashi, A., and Nakajima, T.: Tropospheric aerosol optical thickness from the GOCART model and comparisons with satellite and sun photometer measurements, J. Atmos. Sci., 59, 461–483, 2002.

Colarco, P., da Silva, A., Chin, M., and Diehl, T.: On-line simulations of global aerosol distributions in the NASA GEOS-4 model and comparisons to satellite and ground-based aerosol optical depth, J. Geophys. Res., 115, D14207, doi:10.1029/2009JD012820, 2010.

Cubison, M. J., Ortega, A. M., Hayes, P. L., Farmer, D. K., Day, D., Lechner, M. J., Brune, W. H., Apel, E., Diskin, G. S., Fisher, J. A., Fuelberg, H. E., Hecobian, A., Knapp, D. J., Mikoviny, T., Riemer, D., Sachse, G. W., Sessions, W., Weber, R. J., Weinheimer, A. J., Wisthaler, A., and Jimenez, J. L.: Effects of aging on organic aerosol from open biomass burning smoke in aircraft and laboratory studies, Atmos. Chem. Phys., 11, 12049–12064, doi:10.5194/acp-11-12049-2011, 2011.

Diehl, T.: Personal communication, available at: http://www-lscedods.cea.fr/aerocom/AEROCOM_HC/readme, 2011.

Diskin, G. S., Podolske, J. R., Sachse, G. W., and Slate, T. A.: Open-path airborne tunable 15 diode laser hygrometer, in: Diode Lasers and Applications in Atmospheric Sensing, edited by: Fried, A., SPIE Proc., 4817, 196–204, 2002.

Dunlea, E. J., DeCarlo, P. F., Aiken, A. C., Kimmel, J. R., Peltier, R. E., Weber, R. J., Tomlinson, J., Collins, D. R., Shinozuka, Y., McNaughton, C. S., Howell, S. G., Clarke, A. D., Emmons, L. K., Apel, E. C., Pfister, G. G., van Donkelaar, A., Martin, R. V., Millet, D. B., Heald, C. L., and Jimenez, J. L.: Evolution of Asian aerosols during transpacific transport in INTEX-B, Atmos. Chem. Phys., 9, 7257–7287, doi:10.5194/acp-9-7257-2009, 2009.

Eckhardt, S., Stohl, A., Beirle, S., Spichtinger, N., James, P., Forster, C., Junker, C., Wagner, T., Platt, U., and Jennings, S. G.: The North Atlantic Oscillation controls air pollution transport to the Arctic, Atmos. Chem. Phys., 3, 1769–1778, doi:10.5194/acp-3-1769-2003, 2003.

Flanner, M. G., Zender, C. S., Randerson, J. T., and Rasch, P. J.: Present day climate forcing and response from black carbon in snow, J. Geophys. Res., 112, D11202, doi:10.1029/2006JD008003, 2007.

Fisher, J. A., Jacob, D. J., Purdy, M. T., Kopacz, M., Le Sager, P., Carouge, C., Holmes, C. D., Yantosca, R. M., Batchelor, R. L., Strong, K., Diskin, G. S., Fuelberg, H. E., Holloway, J. S., Hyer, E. J., McMillan, W. W., Warner, J., Streets, D. G., Zhang, Q., Wang, Y., and Wu, S.: Source attribution and interannual variability of Arctic pollution in spring constrained by air-

ACPD
12, 8823–8855, 2012

craft (ARCTAS, ARCPAC) and satellite (AIRS) observations of carbon monoxide, Atmos. Chem. Phys., 10, 977–996, doi:10.5194/acp-10-977-2010, 2010.
Fisher, J. A., Jacob, D. J., Wang, Q., Bahreini, R., Carouge, C. C., Cubison, M. J., Dibb, J. E., Diehl, T., Jimenez, J. L., Leibensperger, E. M., Meinders, M. B. J., Pye, H. O. T., Quinn, P. K., Sharma, S., van Donkelaar, A., and Yantosca, R. M.: Sources, distribution, and acidity of sulfate-ammonium aerosol in the Arctic in winter-spring, Atmos. Environ., 39, 7301–7318, doi:10.1016/j.atmosenv.2011.08.030, 2011.
Fuelberg, H. E., Harrigan, D. L., and Sessions, W.: A meteorological overview of the ARCTAS 2008 mission, Atmos. Chem. Phys., 10, 817–842, doi:10.5194/acp-10-817-2010, 2010.
Harrigan, D. L., Fuelberg, H. E., Simpson, I. J., Blake, D. R., Carmichael, G. R., and Diskin, G. S.: Anthropogenic emissions during Arctas-A: mean transport characteristics and regional case studies, Atmos. Chem. Phys., 11, 8677–8701, doi:10.5194/acp-11-8677-2011, 2011.
Hecobian, A., Liu, Z., Hennigan, C. J., Huey, L. G., Jimenez, J. L., Cubison, M. J., Vay, S., Diskin, G. S., Sachse, G. W., Wisthaler, A., Mikoviny, T., Weinheimer, A. J., Liao, J., Knapp, D. J., Wennberg, P. O., Kürten, A., Crounse, J. D., Clair, J. St., Wang, Y., and Weber, R. J.: Comparison of chemical characteristics of 495 biomass burning plumes intercepted by the NASA DC-8 aircraft during the ARCTAS/CARB-2008 field campaign, Atmos. Chem. Phys., 11, 13325–13337, doi:10.5194/acp-11-13325-2011, 2011.
Hegg, D. A., Warren, S. G., Grenfell, T. C., Doherty, S. J., Larson, T. V., and Clarke, A. D.: Source attribution of black carbon in arctic snow, Environ. Sci. Technol., 43, 4016–4021, doi:10.1021/es803623f, 2009.
Heintzenberg, J.: Arctic Haze: air pollution in polar regions, Ambio, 18, 50–55, 1989.
Huey, L. G., Tanner, D. J., Slusher, D. L., Dibb, J. E., Arimoto, R., Chen, G., Davis, D., Buhr, M. P., Nowak, J. B., Mauldin III, R. L., Eisele, F. L., and Kosciuch, E.: CIMS measurements of HNO_3 and SO_2 at the South Pole during ISCAT 2000, Atmos. Environ., 38, 5411–5421, 2004.
Jacob, D. J., Crawford, J. H., Maring, H., Clarke, A. D., Dibb, J. E., Emmons, L. K., Ferrare, R. A., Hostetler, C. A., Russell, P. B., Singh, H. B., Thompson, A. M., Shaw, G. E., McCauley, E., Pederson, J. R., and Fisher, J. A.: The Arctic Research of the Composition of the Troposphere from Aircraft and Satellites (ARCTAS) mission: design, execution, and first results, Atmos. Chem. Phys., 10, 5191–5212, doi:10.5194/acp-10-5191-2010, 2010.

ACPD
12, 8823–8855, 2012

Koch, D. and Hansen, J.: Distant origins of Arctic black carbon: a Goddard Institute for Space Studies ModelE experiment, J. Geophys. Res., 110, D04204, doi:10.1029/2004JD005296, 2005.

Kondo, Y., Matsui, H., Moteki, N., Sahu, L., Takegawa, N., Kajino, M., Zhao, Y., Cubison, M. J., Jimenez, J. L., Vay, S., Diskin, G. S., Anderson, B., Wisthaler, A., Mikoviny, T., Fuelberg, H. E., Blake, D. R., Huey, G., Weinheimer, A. J., Knapp, D. J., and Brune, H.: Emissions of black carbon, organic, and inorganic aerosols from biomass burning in North America and Asia in 2008, Geophys. Res., 116, D08204, doi:10.1029/2010JD015152, 2011a.

Kondo, Y., Sahu, L., Moteki, N., Khan, F., Takegawa, N., Liu, X., Koike, M., and Miyakawa, T. Consistency and traceability of black carbon measurements made by laser induced incandescence, thermal optical transmittance, and filter-based photo-absorption techniques, Aerosol Sci. Technol., 45(2), 295–312, 2011b.

Kopacz, M., Jacob, D. J., Fisher, J. A., Logan, J. A., Zhang, L., Megretskaia, I. A., Yantosca, R. M., Singh, K., Henze, D. K., Burrows, J. P., Buchwitz, M., Khlystova, I., McMillan, W. W., Gille, J. C., Edwards, D. P., Eldering, A., Thouret, V., and Nedelec, P.: Global estimates of CO sources with high resolution by adjoint inversion of multiple satellite datasets (MOPITT, AIRS, SCIAMACHY, TES), Atmos. Chem. Phys., 10, 855–876, doi:10.5194/acp-10-855-2010, 2010.

Matsui, H., Kondo, Y., Moteki, N., Takegawa, N., Sahu, L. K., Zhao, Y., Fuelberg, H. E., Sessions, W. R., Diskin, G., Blake, D. R., Wisthaler, A., and Koike, M.: Seasonal variation of the transport of black carbon aerosol from the Asian continent to the Arctic during the ARCTAS aircraft campaign, J. Geophys. Res., 116, D05202, doi:10.1029/2010JD015067, 2011a.

Matsui, H., Kondo, Y., Moteki, N., Takegawa, N., Sahu, L. K., Koike, M., Zhao, Y., Fuelberg, H. E., Sessions, W. R., Diskin, G., Anderson, B. E., Blake, D. R., Wisthaler, A., Cubison, M. J., and Jimenez, J. L.: Accumulation-mode aerosol number concentrations in the Arctic during the ARCTAS aircraft campaign: long-range transport of polluted and clean air from the Asian continent, J. Geophys. Res., 116, D20217, doi:10.1029/2011JD016189, 2011b.

McMillan, W. W., Barnet, C., Strow, L. M., Chahine, M., Warner, J., McCourt, M., Novelli, P., Korontzi, S., Maddy, E., and Datta, S.: Daily global maps of carbon monoxide from NASA's Atmospheric InfraRed Sounder, Geophys. Res. Lett., 32, L11801, doi:10.1029/2004GL021821, 2005.

McMillan, W. W., Evans, K. D., Barnet, C. D., Maddy, E. S., Sachse, G. W., and Diskin, G. S.: Validating the AIRS Version 5 CO retrieval with DACOM in situ mea-

ACPD
12, 8823–8855, 2012

surements during INTEX-A and -B, IEEE T. Geosci. Remote Sens., 49(7), 2802–2813, doi:10.1109/TGRS.2011.2106505, 2011.

McNaughton, C. S., Clarke, A. D., Freitag, S., Kapustin, V. N., Kondo, Y., Moteki, N., Sahu, L., Takegawa, N., Schwarz, J. P., Spackman, J. R., Watts, L., Diskin, G., Podolske, J., Holloway, J. S., Wisthaler, A., Mikoviny, T., de Gouw, J., Warneke, C., Jimenez, J., Cubison, M., Howell, S. G., Middlebrook, A., Bahreini, R., Anderson, B. E., Winstead, E., Thornhill, K. L., Lack, D., Cozic, J., and Brock, C. A.: Absorbing aerosol in the troposphere of the Western Arctic during the 2008 ARCTAS/ARCPAC airborne field campaigns, Atmos. Chem. Phys., 11, 7561–7582, doi:10.5194/acp-11-7561-2011, 2011.

Moteki, N. and Kondo, Y.: Effects of mixing state on black carbon measurements by laser-induced incandescence, Aerosol Sci. Technol., 41(4), 398–417, doi:10.1080/02786820701199728, 2007.

Pan, L., Edwards, D. P., Gille, J. C., Smith, M. W., and Drummond, J. R.: Satellite remote sensing of tropo- spheric CO and CH_4: Forward model studies of the MOPIT-T instrument, Appl. Opt., 34, 6976, 1995.

Quinn, P. K., Shaw, G., Andrews, E., Dutton, E. G., Ruoho-Airola, T., and Gong, S. L.: Arctic haze: current trends and knowledge gaps, Tellus B, 59, 99–114, doi:10.1111/j.1600-0889.2006.00238.x, 2007.

Quinn, P. K., Bates, T. S., Baum, E., Doubleday, N., Fiore, A. M., Flanner, M., Fridlind, A., Garrett, T. J., Koch, D., Menon, S., Shindell, D., Stohl, A., and Warren, S. G.: Short-lived pollutants in the Arctic: their climate impact and possible mitigation strategies, Atmos. Chem. Phys., 8, 1723–1735, doi:10.5194/acp-8-1723-2008, 2008.

Raatz, W. E. and Shaw, G. E.: Long-range tropospheric transport of pollution aerosols into the Alaskan Arctic, J. Appl. Meteorol., 23, 1052–1064, 1984.

Rahn, K. A.: Relative importances of North America and Eurasia as sources of arctic aerosol, Atmos. Environ., 15, 1447–1455, 1981.

Rienecker, M. M., Suarez, M. J., Todling, R., Bacmeister, J., Takacs, L., Liu, H.-C., Gu, W., Sienkiewicz, M., Koster, R. D., Gelaro, R., Stajner, I., and Nielsen, E.: The GEOS-5 Data Assimilation System – Documentation of Versions 5.0.1, 5.1.0, and 5.2.0. Technical Report Series on Global Modeling and Data Assimilation 104606, v27, NASA/TM-2008-104606, 2008.

Rienecker, M. M., Suarez, M. J., Gelaro, R., Todling, R., Bacmeister, J., Liu, E., Bosllovich, M. G., Schubert, S. D., Takacs, L., Kim, G. K., Bloom, S., Chen, J., Collins, D., Conaty, A.,

ACPD
12, 8823–8855, 2012

Da Silva, A., Gu, W., Joiner, J., Koster, R. D., Lucchesi, R., Molod, A., Owens, T., Pawson, S., Pegion, P., Redder, C. R., Reichle, R., Robertson, F. R., Ruddick, A. G., Sienkiewicz, M., and Woollen, J.: MERRA: NASA's modern-era retrospective analysis for research and applications, J. Climate, 24, 3624–3648, 2011.

Sachse, G. W., Hill, G. F., Wade, L. O., and Perry, M. G.: Fast response, high precision carbon monoxide sensor using a tunable diode laser absorption technique, J. Geophys. Res., 92, 2071–2081, 1987.

Salcedo, D., Villalta, P. W., Varutbangkul, V., Wormhoundt, J. C., Miake-Lye, R. C., Worsnop, D. R., Ballenthin, J. O., Thorn, W. F., Viggiano, A. A., Miller, T. M., Flagan, R. C., and Seinfeld, J. H.: Effect of relative humidity on the detection of sulfur dioxide and sulfuric acid using a chemical ionization mass spectrometer, J. Mass. Spectr., 231, 17–30, 2004.

Scheuer, E., Talbot, R. W., Dibb, J. E., Seid, G. K., de Bell, L., and Lefer, G.: Seasonal distributions of fine aerosol sulfate in the North American Arctic Basin during TOPSE, J. Geophys. Res., 108, 8370, doi:10.1029/2001JD001364, 2003.

Shaw, G. E.: The Arctic haze phenomenon, B. Am. Meteorol. Soc., 76, 2403–2413, 1995.

Shindell, D. T., Chin, M., Dentener, F., Doherty, R. M., Faluvegi, G., Fiore, A. M., Hess, P., Koch, D. M., MacKenzie, I. A., Sanderson, M. G., Schultz, M. G., Schulz, M., Stevenson, D. S., Teich, H., Textor, C., Wild, O., Bergmann, D. J., Bey, I., Bian, H., Cuvelier, C., Duncan, B. N., Folberth, G., Horowitz, L. W., Jonson, J., Kaminski, J. W., Marmer, E., Park, R., Pringle, K. J., Schroeder, S., Szopa, S., Takemura, T., Zeng, G., Keating, T. J., and Zuber, A.: A multi-model assessment of pollution transport to the Arctic, Atmos. Chem. Phys., 8, 5353–5372, doi:10.5194/acp-8-5353-2008, 2008.

Shinozuka, Y., Redemann, J., Livingston, J. M., Russell, P. B., Clarke, A. D., Howell, S. G., Freitag, S., O'Neill, N. T., Reid, E. A., Johnson, R., Ramachandran, S., McNaughton, C. S., Kapustin, V. N., Brekhovskikh, V., Holben, B. N., and McArthur, L. J. B.: Airborne observation of aerosol optical depth during ARCTAS: vertical profiles, inter-comparison and fine-mode fraction, Atmos. Chem. Phys., 11, 3673–3688, doi:10.5194/acp-11-3673-2011, 2011.

Shinozuka, Y. and Redemann, J.: Horizontal variability of aerosol optical depth observed during the ARCTAS airborne experiment, Atmos. Chem. Phys., 11, 8489–8495, doi:10.5194/acp-11-8489-2011, 2011.

Singh, H. B., Anderson, B. E., Brune, W. H., Cai, C., Cohen, R. C., Crawford, J. H., Cubison, M. J., Czech, E. P., Emmons, L., Fuelberg, H. E., Huey, G., Jacob, D. J., Jimenez, J. L., Kaduwela, A., Kondo, Y., Mao, J., Olson, J. R., Sachse, G. W., Vay, S. A., Weinheimer, A.,

ACPD
12, 8823–8855, 2012

Wennberg, P. O., Wisthaler, A., and ARCTAS Science Team: Pollution influences on atmospheric composition and chemistry at high northern latitudes: boreal and California forest fire emissions, Atmos. Environ., 44, 4553–4564, doi:10.1016/j.atmosenv.2010.08.026, 2010.

Slusher, D. L., Huey, L. G., Tanner, D. J. Flocke, F. M., and Roberts, J. M.: A thermal dissociation-chemical ionization mass spectrometry (TD-CIMS) technique for the simultaneous measurement of peroxyacyl nitrates and dinitrogen pentoxide, J. Geophys. Res., 109, D19315, doi:10.1029/2004JD004670, 2004.

Soja, A. J., Stocks, B., Maczek, P., Fromm, M., Servranckx, R., Turetsky, M., and Benscoter, B.: ARCTAS: the perfect smoke, Canad. Smoke Newslett., 2–7, 2008.

Stohl, A.: Characteristics of atmospheric transport into the Arctic troposphere, J. Geophys. Res., 111, D11306, doi:10.1029/2005JD006888, 2006.

Stohl, A., Berg, T., Burkhart, J. F., Fjæraa, A. M., Forster, C., Herber, A., Hov, Ø., Lunder, C., McMillan, W. W., Oltmans, S., Shiobara, M., Simpson, D., Solberg, S., Stebel, K., Ström, J., Tørseth, K., Treffeisen, R., Virkkunen, K., and Yttri, K. E.: Arctic smoke – record high air pollution levels in the European Arctic due to agricultural fires in Eastern Europe in spring 2006, Atmos. Chem. Phys., 7, 511–534, doi:10.5194/acp-7-511-2007, 2007.

Susskind, J., Barnet, C. D., and Blaisdell, J. M.: Retrieval of atmospheric and surface parameters from AIRS/AMSU/HSB data in the presence of clouds, IEEE Trans. Geosci. Remote Sens., 41, 390–409, 2003.

Wang, Q., Jacob, D. J., Fisher, J. A., Mao, J., Leibensperger, E. M., Carouge, C. C., Le Sager, P., Kondo, Y., Jimenez, J. L., Cubison, M. J., and Doherty, S. J.: Sources of carbonaceous aerosols and deposited black carbon in the Arctic in winter-spring: implications for radiative forcing, Atmos. Chem. Phys., 11, 12453–12473, doi:10.5194/acp-11-12453-2011, 2011.

Warneke, C., Bahreini, R., Brioude, J., Brock, C. A., de Gouw, J. A., Fahey, D. W., Froyd, K. D., Holloway, J. S., Middlebrook, A., Miller, L., Montzka, S., Murphy, D. M., Peischl, J., Ryerson, T. B., Schwarz, J. P., Spackman, J. R., and Veres, P.: Biomass burning in Siberia and Kazakhstan as an important source for haze over the Alaskan Arctic in April 2008, Geophys. Res. Lett., 36, L02813. doi:10.1029/2008GL036194, 2009.

Warneke, C., Froyd, K. D., Brioude, J., Bahreini, R., Brock, C. A., Cozic, J., de Gouw, J. A., Fahey, D. W., Ferrare, R., Holloway, J. S., Middlebrook, A. M., Miller, L., Montzka, S., Schwarz, J. P., Sodemann, H., Spackman, J. R., and Stohl, A.: An important contribution to springtime Arctic aerosol from biomass burning in Russia, Geophys. Res. Lett., 37, L01801, doi:10.1029/2009GL041816, 2010.

ACPD
12, 8823–8855, 2012

Warner, J. X., Comer, M. M., Barnet, C. D., McMillan, W. W., Wolf, W., Maddy, E., and Sachse, G.: A comparison of satellite tropospheric carbon monoxide measurements from AIRS and MOPITT during INTEX-A, J. Geophys. Res., 112, D12S17, doi:10.1029/2006JD007925, 2007.

Warner, J. X., Wei, Z., Strow, L. L., Barnet, C. D., Sparling, L. C., Diskin, G., and Sachse, G.: Improved agreement of AIRS tropospheric carbon monoxide products with other EOS sensors using optimal estimation retrievals, Atmos. Chem. Phys., 10, 9521–9533, doi:10.5194/acp-10-9521-2010, 2010.

Weber, R. J., Orsini, D., Wang, B., Scheuer, E., Talbot, R. W., Dibb, J. E., Seid, G. K., DeBell, L., Mauldin, R. L., Kosciuch, E., Cantrell, C., and Eisele, F.: Investigations into free tropospheric new particle formation in the central Canadian arctic during the winter/spring transition as part of TOPSE, J. Geophys. Res., 108(D4), 8357, doi:10.1029/2002JD002239, 2003.

Zhang, Q., Streets, D. G., Carmichael, G. R., He, K. B., Huo, H., Kannari, A., Klimont, Z., Park, I. S., Reddy, S., Fu, J. S., Chen, D., Duan, L., Lei, Y., Wang, L. T., and Yao, Z. L.: Asian emissions in 2006 for the NASA INTEX-B mission, Atmos. Chem. Phys., 9, 5131–5153, doi:10.5194/acp-9-5131-2009, 2009.

ACPD
12, 8823–8855, 2012

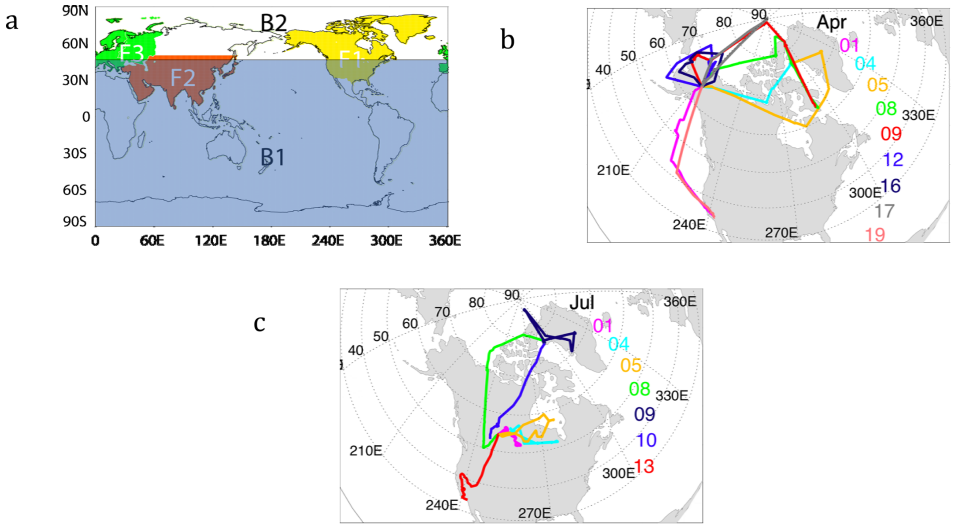

Fig. 1. (a) Regions for tagged CO emissions. In this work, we use 3 tagged fossil fuel CO tracers and 2 tagged biomass burning tracers: F1. North America fossil fuel (NAFF, yellow), F2. Southern Asian fossil fuel (ASFF, red), F3. Europe fossil fuel (EUFF, green), B1. Non-Boreal biomass burning (NBBB, light-blue shaded area), and B2. Boreal biomass burning (BOBB, non-light-blue area). **(b)** and **(c)** NASA DC-8 flight tracks during ARCTAS-A (April based at Fairbank, USA) and ARCTAS-B (July based at Cold Lake, Canada), respectively.

ACPD
12, 8823–8855, 2012

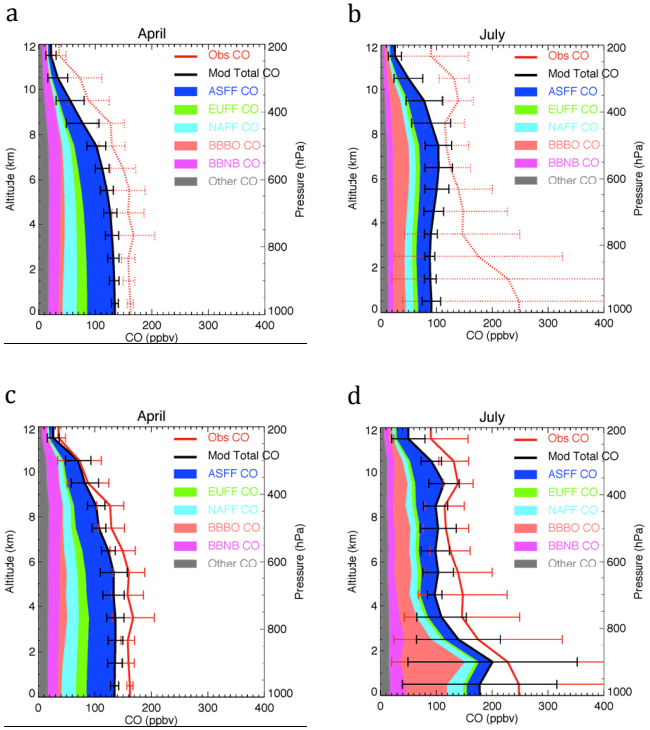

Fig. 2. Vertical distribution of CO volume mixing ratio (ppbv) from DC-8 measurement and GEOS-5 simulation when the GEOS-5 model is the Arctic regional mean over 50° N–90° N and 40° W–170° W for April **(a)** and July **(b)**. The DC-8 CO along flight tracks is shown by the dotted thick red line with standard deviation shown by horizontal bars. GEOS-5 CO is shown by the thick black line for total and by the color shaded areas for the corresponding tag components. The "Other CO" refers to the global CO other than the five tagged COs defined in Fig. 1a. **(c, d)** are similar as **(a, b)** but the GEOS-5 results were sampled by all flights during April ARCTAS-A **(c)** and July ARCTAS-B **(d)** campaigns.

ACPD
12, 8823–8855, 2012

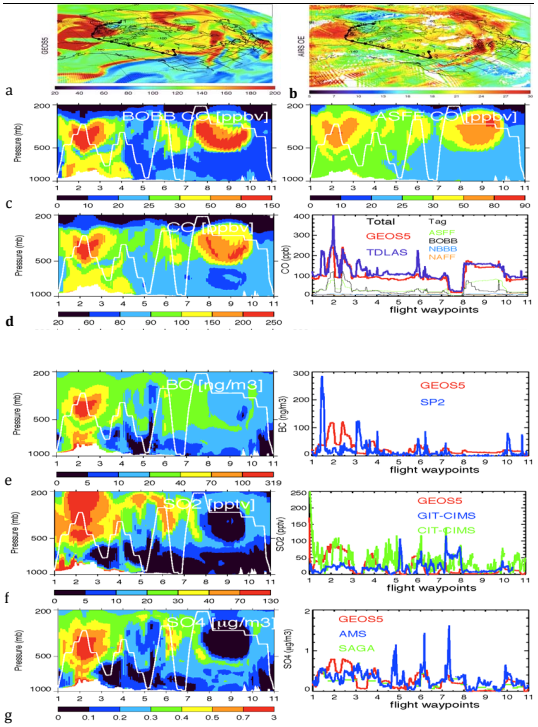

Fig. 3. The modeled and measured CO and aerosols during the ARCTAS flight 21 on 8 July from Cold Lake, Canada, terminating in Thule, Greenland. The CO mixing ratio distribution at 400 hPa from GEOS-5 is shown in **(a)** and the column CO amount ($\times 10^{17}$ molecules cm^{-2}) from AIRS is in **(b)**. The solid line with dots and numbers shows the actual flight track of DC8. **(c)** is the curtain plots for tagged CO to BOBB (left) and ASFF (right), with the white line representing the flight track. **(d)** left shows total CO curtain plot along the flight track and right shows measured and modeled total CO (thick lines) as well as modeled tagged CO (thin lines), during the flight 21. **(e–g)** are similar to **(d)** but for BC, SO_2, and SO_4, respectively.

ACPD
12, 8823–8855, 2012

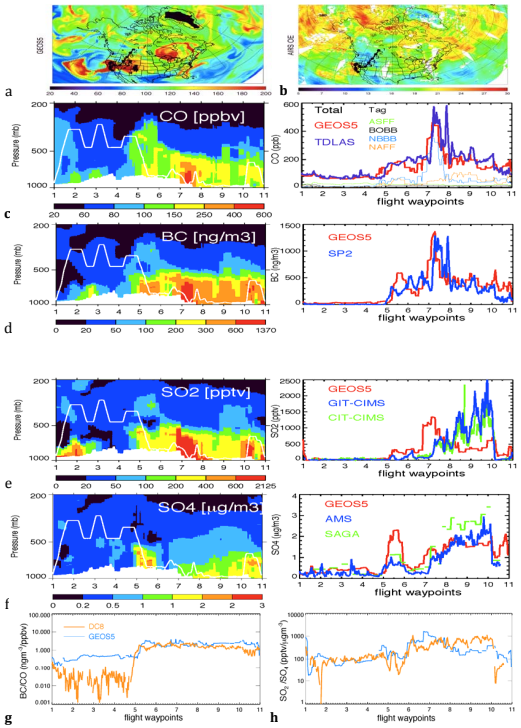

Fig. 4. The modeled and measured CO and aerosols during the ARCTAS flight 24 on 13 July from Cold Lake, Canada returning to Palmdale, Califonia, USA. The CO mixing ratio distribution over 700 hPa from GEOS-5 is shown in **(a)** and the column CO ($\times 10^{17}$ molecules cm^{-2}) from AIRS is shown in **(b)**. The solid line with dots and numbers shows the actual flight track of DC8. **(c)** left shows CO curtain plot along the flight track with the white line representing the flight track and right shows measured and modeled CO (thick lines) as well as modeled tagged CO (thin lines), during the flight. **(d–f)** are similar to **(c)** but for BC, SO_2, and SO_4, respectively. The last panel shows the ratio of BC to CO **(g)** and SO_2 to SO_4 **(h)** along the flight track with yellow line from DC-8 measurements and blue line from GEOS-5 simulation.

ACPD
12, 8823–8855, 2012

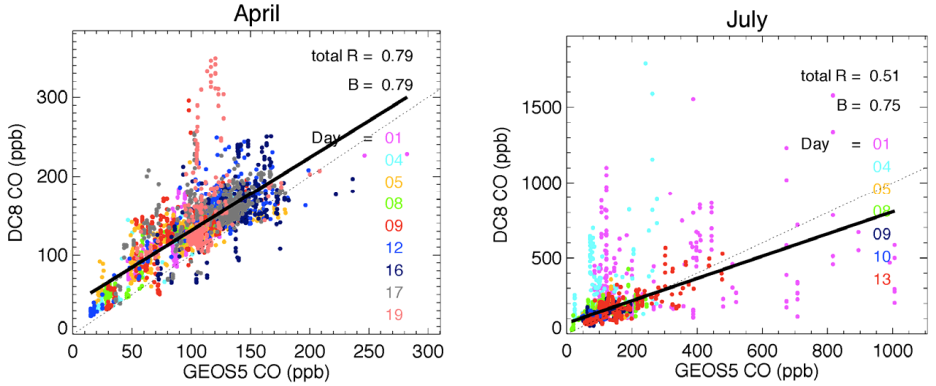

Fig. 5. Scatter plot of CO volume mixing ratio (ppb) from the DC-8 aircraft measurements and the GEOS-5 simulation for April and July, with colored dots for different flights. The thick solid line is the linear regression line and the thin dotted line is 1:1 line. The data correlation coefficient (R) and the ratio (B) of average model and measurement are calculated for each campaign.

ACPD
12, 8823–8855, 2012

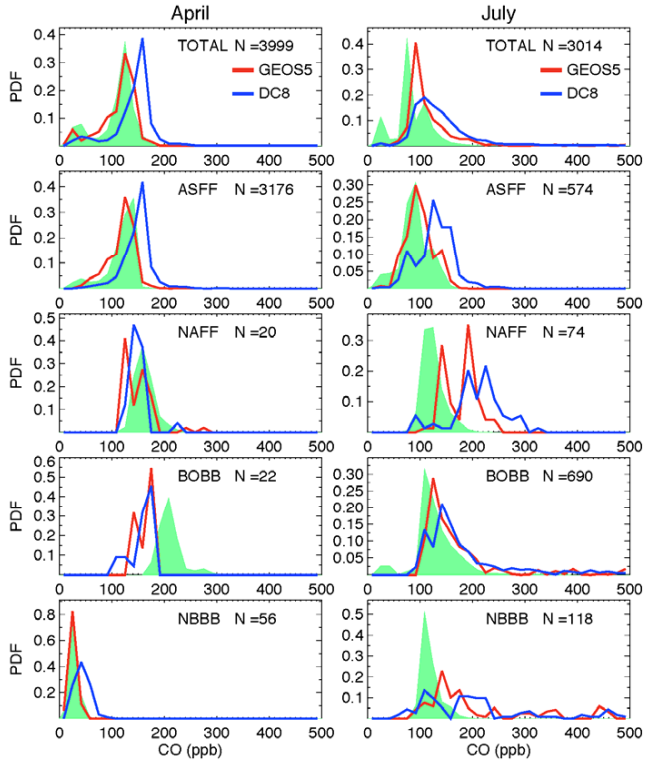

Fig. 6. The probability distribution function (PDF) of total CO over two ARCTAS campaign periods and over the 4 tagged CO categories. The latter is determined by the modeled dominant tag CO (i.e. one of 5 tagged CO explained in Fig. 1a) in air pollution in every 1-min measurement period along the flight track. Please note EUFF is not shown since CO from Europe anthropogenic emission always contributed as background CO to the pollution measured during the ARCTAS campaign. The blue and red lines are the PDFs of DC-8 and GEOS-5 sampled along flight tracks and green areas are the PDFs of GEOS-5 CO over the Arctic region 50° N–90° N and 40° W–170° W and up to 200 hPa. *N* is number of 1-min data point.

ACPD
12, 8823–8855, 2012